IOPscience iopscience.iop.org

Home Search Collections Journals About Contact us My IOPscience

Nanoscale analysis of Ru(0001) oxidation using low-energy and photoemission electron microscopy

This article has been downloaded from IOPscience. Please scroll down to see the full text article.

2009 J. Phys.: Condens. Matter 21 314018

(http://iopscience.iop.org/0953-8984/21/31/314018)

View the table of contents for this issue, or go to the journal homepage for more

Download details:
IP Address: 129.252.86.83
The article was downloaded on 29/05/2010 at 20:40

Please note that terms and conditions apply.

IOP Publishing Journal of Physics: Condensed Matter

J. Phys.: Condens. Matter **21** (2009) 314018 (6pp) doi:10.1088/0953-8984/21/31/314018

Nanoscale analysis of Ru(0001) oxidation using low-energy and photoemission electron microscopy

J I Flege[1] **and P Sutter**

Center for Functional Nanomaterials, Brookhaven National Laboratory, Upton, NY 11973, USA

E-mail: flege@ifp.uni-bremen.de

Received 4 January 2009, in final form 16 March 2009
Published 7 July 2009
Online at stacks.iop.org/JPhysCM/21/314018

Abstract

CO oxidation over oxygen-rich Ru(0001) surfaces is one of the most studied catalytic oxidation reactions in surface science and of widespread interest as a model system for the redox chemistry of transition metal model catalysts. Here, we present an extensive low-energy electron microscopy (LEEM) and photoemission electron microscopy study of the oxidation of Ru(0001), which constitutes a crucial step in understanding the overall surface reaction. After characterizing the different surface nanoscale morphologies observed depending on the oxidation temperature, three distinct oxygen-rich phases are identified by dark-field microscopy and local valence-band spectroscopy. Furthermore, *in situ* LEEM allows us to follow the growth of single rutile oxide nuclei in real time and determine the relevant activation barriers that induce quasi-one-dimensional growth of oxide nanorods, whose growth rate is limited by O incorporation.

(Some figures in this article are in colour only in the electronic version)

1. Introduction

The (0001) surface of ruthenium is one of the best studied transition metal surfaces and has become a model system for this entire class of materials regarding their general chemical and catalytic properties as, e.g., in CO oxidation, the simplest oxidation reaction. Although much is already known from extensive experimental and theoretical studies (see, e.g., [1] for a recent review), the ongoing controversy [2–4] regarding the catalytically active phases and prevailing mechanisms for CO oxidation has sparked renewed interest, and it clearly demonstrates the demand for additional studies.

Recently [5], we addressed a crucial aspect of all catalytic oxidation reactions over Ru(0001), namely the oxidation of the substrate, using intensity–voltage low-energy electron microscopy (IV-LEEM), where we showed the coexistence of two competing oxygen-rich phases after prolonged exposure to NO_2, i.e. the bulk-like rutile $RuO_2(110)$ thin-film oxide and a trilayer-like O–Ru–O surface oxide, which independently evolve from the (1×1)-O chemisorption phase. In the present LEEM and photoemission electron microscopy (PEEM) study, we characterize the relevant temperature regimes that lead to qualitative differences in the morphology of the oxidized Ru(0001) surface. The coexisting oxygen-rich phases are identified by dark-field microscopy and acquisition of local valence-band spectra and subsequent comparison to calculated partial densities of states based on density functional theory (DFT) calculations for oxygen-rich trial structures [6]. One of the most prominent characteristics of the thin-film rutile oxide RuO_2 is quasi-one-dimensional growth on the nanoscale in the whole temperature regime investigated, and we analyse its nanoscale oxidation kinetics *in situ* and *in real time* depending on temperature and oxygen supply, allowing for the determination of the activation barriers and rate-limiting steps in the oxidation process.

2. Experimental details

All experiments were performed at the Center for Functional Nanomaterials (CFN) at Brookhaven National Laboratory in

[1] Present address: Institute of Solid State Physics, University of Bremen, 28359 Bremen, Germany.

 © 2009 IOP Publishing Ltd Printed in the UK

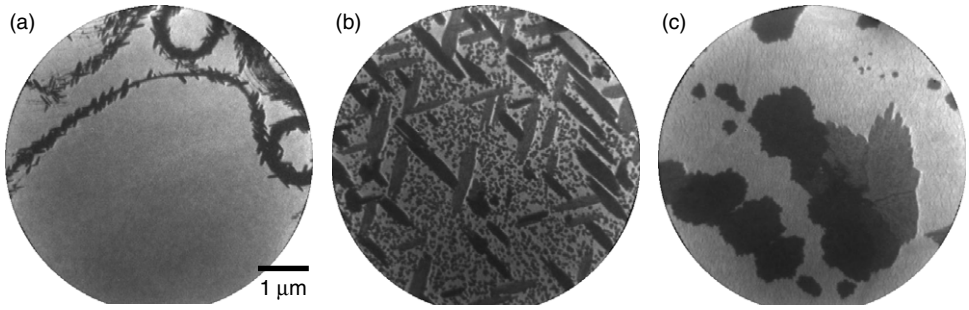

Figure 1. Low-energy electron micrographs ($E = 6$ eV) demonstrating the influence of temperature on surface morphology for oxidation at a NO_2 pressure of $p = 6\times10^{-7}$ Torr. (a) $T = 620$ K (b), $T = 730$ K, (c) $T = 800$ K.

Upton, NY (USA). Photoemission microscopy data were obtained using the newly commissioned low-energy and photoemission electron microscope [7] installed at beamline U5UA of the National Synchrotron Light Source (NSLS). A commercial Ru(0001) crystal (Mateck) oriented to a precision of 0.1° was initially cleaned *ex situ* using repeated oxidation followed by high-temperature annealing under Ar flow before introduction into the ultrahigh-vacuum system of the microscope for further cleaning cycles involving exposure to molecular oxygen and sequential flash-annealing based on well-established procedures [8]. All substrate temperatures were inferred from the reading of a standard W–Re thermocouple spot-welded to the sample support of the holder. For efficient oxidation at near-UHV pressures, the sample was dosed with NO_2, a convenient precursor for atomic oxygen [9], from a leak valve mounted in direct line of sight of the sample surface. The valence-band spectra were obtained in PEEM mode using the first harmonic of the undulator tuned to a primary photon energy of 32 eV and a diffraction grating exhibiting 600 lines mm^{-1} for monochromatization. The data were processed with the Gxsm software developed by Zahl *et al* [10] and the program ImageJ [11].

3. Results and discussion

3.1. Oxygen-rich surface morphologies

Figure 1 displays LEEM images acquired after exposure to NO_2 at a partial pressure of 6×10^{-7} Torr for different sample temperatures employed during oxidation. After dosing at 620 K (a), oxidation is only witnessed at the step bunches of the Ru substrate, which provide efficient pathways for facile oxygen incorporation, and therefore act as nucleation centres for the oxygen-rich phases, which appear in dark contrast at an electron energy of 6 eV. If, however, the substrate temperature is raised to about 730 K, nucleation of oxide patches is observed at both step edges and terraces (b). Close inspection shows a coexistence of anisotropic island shapes oriented along the main crystallographic directions of the hexagonal Ru(0001) surface with small irregular islands randomly distributed over the terraces. Comparing to the lower temperature reveals that the same shape anisotropy of the islands is already visible at 620 K, although on a smaller length scale. This pronounced mesoscale orientational anisotropy is lifted at yet higher temperatures, as illustrated for $T = 800$ K in figure 1(c). In this regime, large and mostly isotropic islands are observed, along with some internal structure, which is attributed to grain boundaries, indicating that these islands evolved from multiple nuclei. Concluding this section on the temperature regimes, we note that the 'mesoscale patterns' observed here are very similar to what has been found in an earlier PEEM study [12, 13], which, however, lacked the required spatial and temporal resolution to relate these findings to the underlying oxidation mechanism, which will be addressed by *in situ* LEEM oxidation experiments in section 3.3.

3.2. Island identification by dark-field LEEM and local spectroscopy

Due to the different crystallographic symmetry and properties of the hexagonally close-packed Ru(0001) substrate and the well-known rutile $RuO_2(110)$ phase, which is known to form upon sufficient exposure to oxygen [14, 15], an unambiguous identification of the island nature is achievable by dark-field microscopy. In figure 2(a), a typical low-energy electron diffraction (LEED) pattern is shown after oxidation of the clean Ru(0001) surface at 730 K with NO_2 at a partial pressure of 6×10^{-7} Torr. While the reflection spots marked (10) and (01) form the (1×1) unit mesh attributed to the (1×1)-O reconstruction, the remaining peaks arise from an advanced oxidation state of the Ru(0001) surface. The association with structural features visible in LEEM is straight-forward by sequentially employing the spots labelled 'A', 'B', and 'C' in dark-field microscopy. In figure 2(b), all three false colour coded dark-field images are superimposed to form a composite LEEM image, in which all islands exhibiting anisotropic shapes are clearly reproduced. Since 'A', 'B', and 'C' represent the (01) reflections of the three rotational domains of the rutile unit mesh [15], all islands oriented along a distinct crystallographic direction exhibit the same false colour contrast in figure 2(b) and are readily identified as individual rotational domains of thin-film $RuO_2(110)$. Analogously, all other reflection spots visible in figure 2(a) can be explained by the superposition of both the hexagonal (1×1)-O chemisorbed phase and the rectangular (1×1) unit mesh of the rutile $RuO_2(110)$ phase.

Although the composite dark-field image from figure 2(b) and the bright-field image displayed in figure 1(b) do not

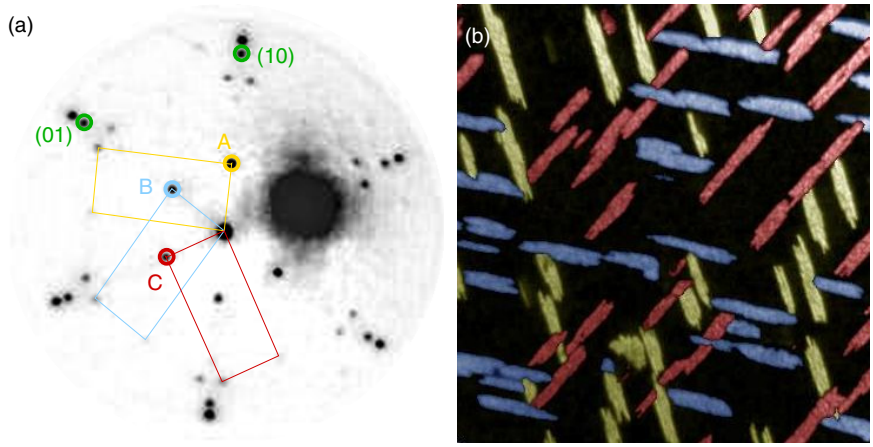

Figure 2. Low-energy electron diffraction pattern (a) and three superimposed dark-field LEEM images (b) after oxidation at a NO_2 pressure of $p = 6\times10^{-7}$ Torr. The three rotational domains are colour coded in reciprocal (a) and real (b) space.

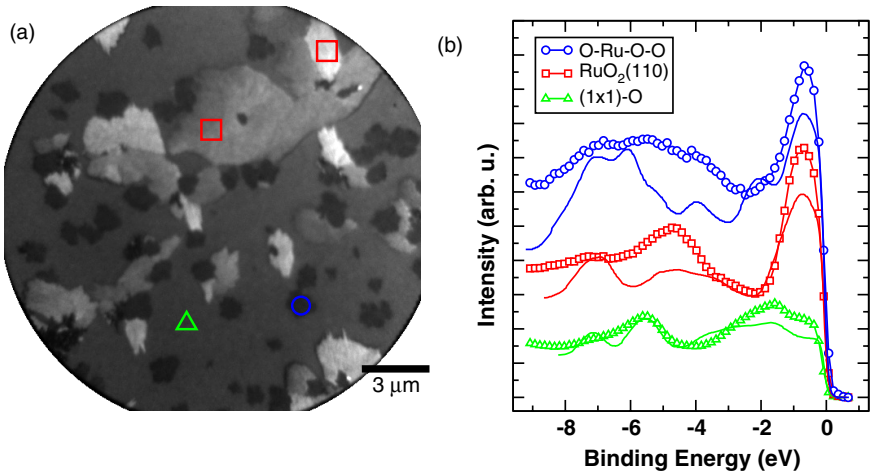

Figure 3. Low-energy ($E = 17$ eV) electron micrograph (a) and local valence-band spectra (b) for the (1 × 1)-O (△), $RuO_2(110)$ (□), and O–Ru–O (○) phases after oxidation at a NO_2 pressure of $p = 2\times10^{-7}$ Torr. Corresponding areas and spectra are marked by the same symbols.

show identical surface areas, but surface regions subjected to identical oxidation conditions, a qualitative comparison between them indicates that the small round-shaped islands apparently do not contribute to the diffracted intensities of the rutile structure, strongly suggesting a different local atomic structure for this oxygen-rich phase. Indeed, by virtue of dynamic IV-LEEM experiments in connection with multiple-scattering LEED calculations the coexistence of *three* distinct surface phases can be established, as described in a related study by the present authors [5]. Based on the reported findings, it was concluded that, in addition to the (1 × 1)-O and $RuO_2(110)$ surface phases, a poorly ordered surface oxide exists, which essentially resembles an O–Ru–O trilayer-like structure, whose existence was previously predicted based on DFT [16]. Here, we follow a different approach in characterizing and possibly identifying the individual structural components present after prolonged oxidation by analysing their phase-specific electronic valence-band structure and comparing them with calculated partial densities of states (pDOS) for a set of oxygen-rich trial structures from the literature [6]. For this purpose, oxidation has been performed at higher temperature (790 K) and slightly reduced NO_2 pressure (2×10^{-7} Torr), resulting in generally larger islands and a lower island density (see figure 3(a)). This way, large and spectroscopically uniform areas are created, allowing for averaging over large, structurally equivalent surface areas for the extraction of high-quality local spectra from a stack of PEEM images. The local valence-band spectra shown in figure 3(b), however, are truly representative for the individual oxygen-rich phases regardless of the precise oxidation conditions since they were found to remain virtually unchanged even for small nanoscale islands, which were analysed after oxidation at 710 K in separate PEEM experiments.

The valence-band spectra of the different surface components are displayed in figure 3(b) along with the published 4d pDOS, which were calculated for the first layer Ru atoms of the DFT-relaxed oxygen-rich structures [6]. Quite strikingly, both the pDOS of the first layer Ru atoms in the (1 × 1)-O adlayer and the $RuO_2(110)$ thin-film oxide closely resemble the corresponding experimental spectra with respect

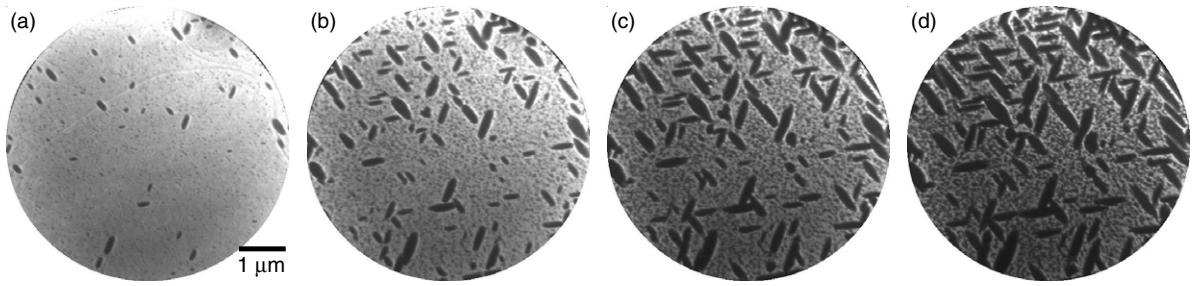

Figure 4. Low-energy electron micrographs ($E = 6$ eV) for different NO_2 doses acquired during oxidation at $p = 6\times10^{-7}$ Torr and substrate temperature $T = 710$ K. (a) 50 L, (b) 200 L, (c) 350 L, (d) 500 L.

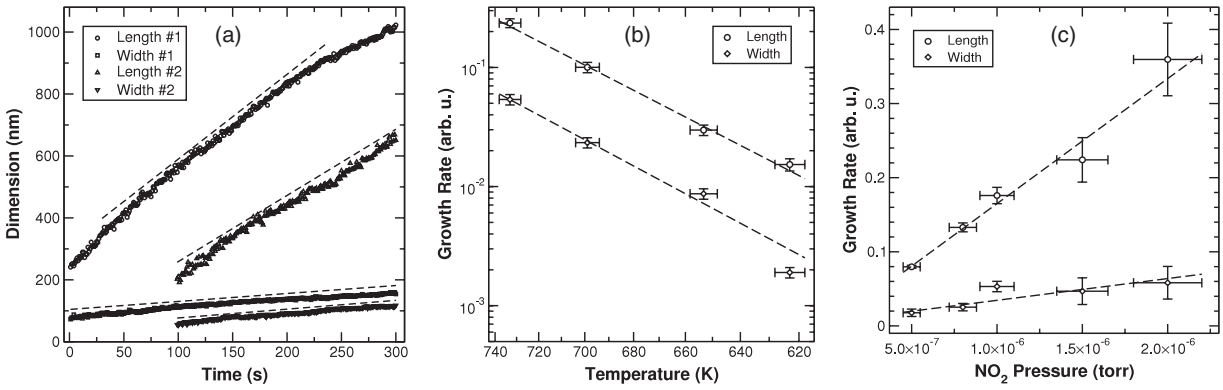

Figure 5. Temporal evolution (a), temperature dependence (b), and pressure dependence (c) of the growth rates of the anisotropic RuO_2 islands measured *in situ* by LEEM.

to the peak positions. Interestingly, the same rutile valence-band structure is observed for surface areas that differ in (00) reflectivity as, e.g., observed for the two regions marked by squares in figure 3(a). However, since both areas exhibit virtually identical intensity–voltage curves (not shown) and valence-band structures, albeit different integral intensities, these findings can be interpreted as indications of different local film thicknesses.

The qualitative match between the experimental spectra and the calculated pDOS establishes the notion of using the experimental valence-band structure as a fingerprint that can be used for structural identification if compared to a catalogue of theoretically determined DOS. When applied to the experimental spectra of the surface oxide, its valence-band structure shows a remarkable agreement with the computed pDOS for the O–Ru–O–O structure, corroborating the previous structural assignment based on IV-LEEM [5]. However, as stated in [6], no distinction between different trilayer-like structures, e.g., the O–Ru–O and the O–Ru–O–O geometry, can be made at this point since both trilayer types exhibit very similar 4d bands.

3.3. Oxidation kinetics and mechanism

After analysing the surface constituents, we now turn to the growth characteristics and the question of the nature of the prevailing oxidation mechanism. For this purpose, the oxidation of the surface was monitored *in situ* by LEEM, which allows an in-depth analysis of the oxide growth kinetics. Figure 4 shows a typical LEEM time-lapse sequence of the evolution of the surface morphology after exposure to NO_2 at a temperature of 710 K. Clearly, the evolution of thin-film oxide and trilayer islands is visible with increasing oxygen dose up to 500 L. From an analysis of the growth of the lengths and widths of the RuO_2 patches as a function of time (NO_2 dose), constant rates are deduced (figure 5(a)). Since the growth rate is much higher for the island length than the width for low to intermediate temperatures, i.e., up to about 750 K, the oxide patches appear to grow in a quasi-one-dimensional fashion. To shed light on the fundamental origin of this finding, we studied the growth rate of the RuO_2 islands at constant NO_2 pressure (5×10^{-7} Torr) as a function of temperature in accompanying experiments (figure 5(b)). Assuming an exponential dependence of the form $\exp(-E_A/k_BT)$, an activation energy E_A of about 1.03 ± 0.05 eV is extracted for both the length and the width. In order to determine the rate-limiting species in the oxidation process, additional experiments were conducted to characterize the dependence of the growth rate on the NO_2 partial pressure (figure 5(c)). As clearly demonstrated by the viewgraph, both the rates for the length and width increase linearly with the oxygen supply, indicating that the attachment and incorporation of oxygen define the rate-limiting step in the oxidation process in this temperature range.

The experimental evidence presented in figure 5 indicates that the observed difference in growth rates is not driven by the underlying kinetics, as can be rationalized in the following way. If there were significant differences in, e.g., the diffusion

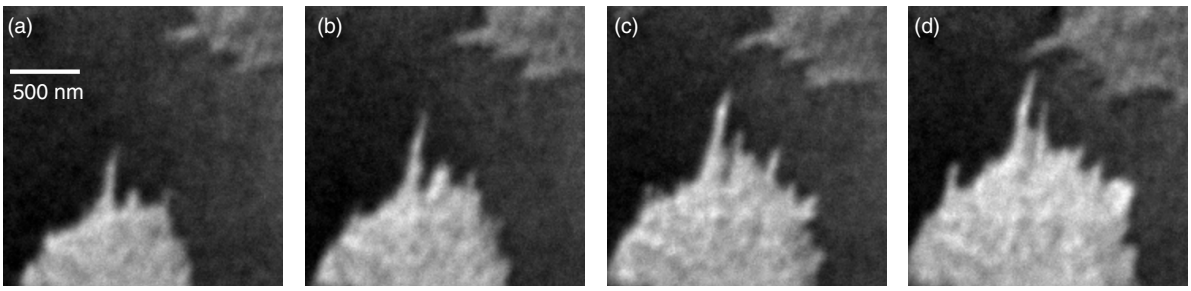

Figure 6. Time-lapse sequence of the finger-like growth of $RuO_2(110)$ at a NO_2 pressure of 2×10^{-7} Torr and a temperature of 775 K. (a) $\Delta t = 0$ s, (b) $\Delta t = 100$ s, (c) $\Delta t = 200$ s, and (d) $\Delta t = 300$ s.

lengths of the oxygen adspecies along the substrate directions or along the island edges, their individual values should vary exponentially with temperature exhibiting a Boltzmann-type behaviour. This would result in an exponential temperature dependence for their ratio, which would in turn induce a temperature-dependent island shape. This prediction, however, is in stark contrast to the unchanged aspect ratio of the islands for the discussed temperature and pressure range.

From an earlier LEED study [15] it is known that the $[\bar{1}10]$ direction of the rutile RuO_2 thin film is oriented along the $[10\bar{1}0]$ main symmetry direction of the Ru(0001) substrate, in agreement with our present results. Likewise, the [001] direction of the rutile unit mesh is oriented along the $[\bar{1}2\bar{1}0]$ direction of the underlying substrate and constitutes the primary growth direction of the oxide grains [12]. While the rutile layer grows along the [001] direction, the 'easy axis', at relatively high velocity, we find here that the growth of the island width is significantly hindered. Nevertheless, for high-temperature growth the shape anisotropy may be lifted on the mesoscale, as illustrated in figure 6 by a time-lapse sequence recorded during oxidation at 775 K and a NO_2 pressure of 2×10^{-7} Torr. Both RuO_2 patches, located in the upper right and the lower left corners, grow in a finger-like fashion along the high-symmetry directions of the substrate, i.e., the [001] direction of the oxide, accompanied by adjacent nucleation of new domains in the perpendicular direction, which probably reflects the strongly increased diffusion lengths for adsorbed oxygen species at this temperature. The 'fingers' appear about 40–50 nm wide, which is close enough to the overall lateral resolution of the microscope to imagine true island shapes of even higher aspect ratio, hence suggesting the term 'oxide nanorods'. Upon further NO_2 dose, these nanorods start to again expand along the respective [001] direction.

While we cannot unambiguously identify the origin of the observed shape anisotropy, kinetic effects do not play a dominating role, and a possible reason seems to be connected to the epitaxial relation to the substrate, which is reflected by the orientational alignment of the RuO_2 grains. Although the rutile oxide grows incommensurately on the hexagonally close-packed metal with in-plane and out-of-plane lattice constants close to the known bulk values for films exceeding a few monolayers, as evidenced from surface x-ray diffraction [17], the relative lattice mismatch along the [001] growth direction is considerably less than in the perpendicular $[\bar{1}10]$ direction, possibly inducing a smaller increase of the interfacial strain energy upon lateral growth. This argument is in line with the observation of an anisotropic partial strain relaxation, i.e., a slight compression of the oxide film in the [001] direction accompanied by an expansion along the $[\bar{1}10]$ direction, which was speculated to be caused by the tendency to minimize the Ru–Ru distances for low-coordinated, ultra-thin oxide layers [18].

In the high-temperature growth regime ($\gtrsim$780 K), the island shapes become more and more isotropic on the mesoscale, as observed previously [13], due to considerably increased nucleation of adjacent oxide islands, representing a rather general kinetic effect in island nucleation, and enhanced formation of rotated domains extending from the same principle island nucleus during lateral growth. However, it should be noted that even in the low to intermediate-temperature regimes, in which almost perfect nanorod growth is observed, the rutile island shapes become irregular once the RuO_2 and O–Ru–O trilayer domains get very close and start competing for the same surface area and abundant oxygen species, thereby blocking and effectively perturbing the one-dimensional growth mode of the thin-film oxide.

4. Conclusion

We have presented an extensive study of the oxidation of the Ru(0001) surface by low-energy electron microscopy and synchrotron-based photoemission electron microscopy. Following the identification of the rutile RuO_2 thin-film oxide and the concurring O–Ru–O trilayer patches, *in situ* LEEM experiments provided detailed insight into the oxidation process, which is shown to be governed by an intricate interplay of energetics and growth kinetics. Accordingly, quasi-one-dimensional growth of oxide nanorods, less than 50 nm wide, along the [001] direction of the rutile oxide domain concurring with competing trilayer formation is responsible for the anisotropic shapes and complex surface patterns observed on a mesoscopic scale.

Acknowledgments

The authors would like to thank Th Schmidt for helpful and stimulating discussions. Work performed under the auspices of the US Department of Energy under contract No. DE-AC02-98CH1-886.

References

[1] Reuter K 2007 Nanometer and subnanometer thin oxide films at surfaces of late transition metals *Nanocatalysis* (*Nanoscience and Technology*) 1st edn (Berlin: Springer) pp 343–76

[2] Goodman D W, Peden C H F and Chen M S 2007 *Surf. Sci.* **601** L124

[3] Over H, Muhler M and Seitsonen A P 2007 *Surf. Sci.* **601** 5659–62

[4] Over H, Balmes O and Lundgren E 2009 *Surf. Sci.* **603** 298–303

[5] Flege J I, Hrbek J and Sutter P 2008 *Phys. Rev.* B **78** 165407

[6] Reuter K, Ganduglia-Pirovano M V, Stampfl C and Scheffler M 2002 *Phys. Rev.* B **65** 165403

[7] Flege J I, Vescovo E, Nintzel G, Lewis L H, Hulbert S and Sutter P 2007 *Nucl. Instrum. Methods Phys. Res.* B **261** 855

[8] Madey T E, Engelhardt H A and Menzel D 1975 *Surf. Sci.* **48** 304

[9] Malik I J and Hrbek J 1992 *J. Vac. Sci. Technol.* A **10** 2565–9

[10] Zahl P, Bierkandt M, Schröder S and Klust A 2003 *Rev. Sci. Instrum.* **74** 1222

[11] Abramoff M, Magelhaes P and Ram S 2004 *Biophoton. Int.* **11** 36

[12] Böttcher A, Krenzer B, Conrad H and Niehus H 2000 *Surf. Sci.* **466** L811

[13] Böttcher A, Krenzer B, Conrad H and Niehus H 2002 *Surf. Sci.* **504** 42

[14] Over H, Kim Y D, Seitsonen A P, Wendt S, Lundgren E, Schmid M, Varga P, Morgante A and Ertl G 2000 *Science* **287** 1474–6

[15] Kim Y D, Seitsonen A P and Over H 2000 *Surf. Sci.* **465** 1–8

[16] Reuter K, Stampfl C, Ganduglia-Pirovano M V and Scheffler M 2002 *Chem. Phys. Lett.* **352** 311–7

[17] He Y B, Knapp M, Lundgren E and Over H 2005 *J. Phys. Chem.* B **109** 21825

[18] Over H, Seitsonen A P, Lundgren E, Schmid M and Varga P 2002 *Surf. Sci.* **515** 143–56